Correlating composition and luminescence in AlInGaN epilayers

P.R. Edwards [a,*], R.W. Martin [a], K. Bejtka [a], K.P. O'Donnell [a], S. Fernández-Garrido [b], E. Calleja [b]

[a] Department of Physics, SUPA, University of Strathclyde, Glasgow G4 0NG, UK

[b] ISOM and Departamento de Ingeniería Electrónica, ETSI Telecomunicacion, Universidad Politécnica de Madrid, 28040 Madrid, Spain

ARTICLE INFO

Article history:
Available online 25 November 2008

Keywords:
AlInGaN
GaN
MBE
Cathodoluminescence
WDX

ABSTRACT

Epilayers of the quaternary alloy $Al_xIn_yGa_{1-x-y}N$ have been grown on GaN/sapphire templates by plasma-assisted molecular beam epitaxy. The emission properties and elemental compositions of these samples were evaluated simultaneously and intercorrelated by combining hyperspectral cathodoluminescence imaging and wavelength-dispersive X-ray mapping. Use was made of inherent variations in growth temperature across a single epilayer to study the resultant effect on the different metal fractions and luminescence emission wavelength. By examining statistical correlations in this data, the interdependence of the fractions of constituent binary compounds, together with the associated changes in emission characteristics, can be clarified without the need to grow a systematic series of samples.

1. Introduction

The quaternary alloy $Al_xIn_yGa_{1-x-y}N$ (hereafter referred to as AlInGaN) holds promise for a number of uses, particularly in applications where it can be lattice-matched to GaN [1,2] with a variable UV band-gap. However, better understanding of the growth mechanism of this material is an essential prerequisite for its technological development, particularly given the conflicting growth conditions required by the constituent binary compounds. Optimisation of growth temperature is crucial since InN requires a relatively low growth temperature, whilst GaN prefers a higher temperature and AlN higher still. Previous work by some of the present authors [3–5] has focused on the analysis of series of samples, each grown under marginally different conditions. In the current work, we exploit the

temperature-induced composition variation commonly present across a single epilayer, combined with a large number of spatially resolved measurements, in order to investigate such variation statistically. This method has been successfully applied to a number of different epilayers, a single example of which is presented in this work.

2. Sample growth

The AlInGaN samples were grown by plasma-assisted molecular beam epitaxy (PA-MBE) in a Riber Compact 21 reactor, using an Addon r.f. plasma N source and Al, Ga and In Knudsen cells. A 100 nm buffer layer of GaN was initially grown at low temperature (730 °C) on a Lumilog *c*-plane GaN-on-sapphire template. This was followed by ≈300 nm of wurtzite AlInGaN grown at a temperature of 595 °C under intermediate metal-rich conditions to ensure a two dimensional growth and to avoid the formation of metal droplets on the surface [5]. The rotation centre during the growth was in the centre of the sample, which was one-quarter of a 2-in. wafer. Due to edge effects, there was a temperature gradient across the sample during growth with a higher temperature close to the edges.

3. Measurement details

The composition and luminescence spectra of the samples were measured in a combined cathodoluminescence (CL) and wavelength-dispersive X-ray (WDX) spectroscopy system. Based on a Cameca SX100 electron probe microanalyser, this instrument makes use of an optical microscope which is co-axial and confocal with the electron beam to collect light emitted from the sample under electron beam excitation [6]. At each point in the rastered scan, a complete room-temperature CL spectrum is recorded using a CCD spectrograph, resulting in a multidimensional data cube, or hyperspectral image. Elemental data is acquired simultaneously using three WDX spectrometers, allowing composition and emission to be mapped together under identical conditions and avoiding issues of position registration which would otherwise arise from use of non-simultaneous *ex-situ* measurements.

Beam parameters were chosen to yield a suitable signal/noise ratio whilst confining the excitation to the quaternary epilayer. The 6 kV, 20 nA beam was held stationary whilst the sample was scanned in 50 μm steps over an area of 4.05 × 9.45 mm, taking 800 ms per pixel. Ga Lα and Al Kα X-rays were detected with WDX spectrometers using thallium acid phthalate (TAP) diffracting crystals, with a pentaerythritol (PET) crystal used to monitor the In Lα line. Twenty points were measured across the sample using fully quantitative WDX (i.e. using standards-based, ZAF-corrected peak-minus-background analysis), and these were used to calibrate the X-ray count maps in terms of AlN, GaN and InN fractions [7]. Nitrogen content was also measured for these points, and the material was confirmed to be stoichiometric at all measured points. Rutherford backscattering spectrometry measurements carried out on similar samples showed good agreement with the WDX analysis [5].

4. Results

Fig. 1 shows the results of mapping the In, Ga and Al X-ray peak counts after scaling them with the quantitative data. The InN and GaN maps clearly show the effect of a growth temperature gradient across the sample, with increasing InN and decreasing GaN content towards the top right of the maps; this corresponds with a lower temperature in this region, which was near the centre of the growth wafer. Little variation in the AlN content is observed; this is despite the fact that it would be expected to show a similar behaviour to GaN, due to near-unity sticking fractions for both Al and Ga in MBE growth in this temperature region. This behaviour is analysed in depth in Ref. [3]. Fig. 2 shows an alternative representation of the composition data, in the form of a ternary plot showing the relative abundance of the three binary compounds in the alloy, in which each point represents one of the 15,580 pixels in the X-ray maps with the sum of the binary compositions set to 100%. The data are seen to form an elongated cluster almost parallel to the lines of constant AlN. There is, however, a slight tendency for the AlN content to increase with increasing GaN, albeit at a slower rate, as illustrated by the major and minor axes of the ellipse.

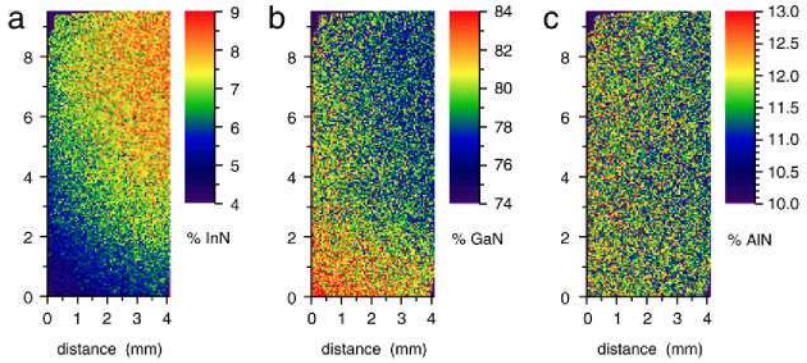

Fig. 1. Maps of (a) In Lα, (b) Ga Lα and (c) Al Kα X-ray counts, scaled to show the local percentage of InN, GaN and AlN respectively.

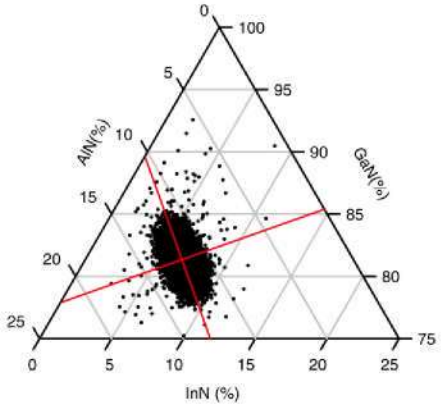

Fig. 2. Ternary diagram showing each pixel from the InN, GaN and AlN maps in Fig. 1 plotted according to their relative abundances.

The room temperature CL acquired concurrently with the WDX data was found to show a single band-edge emission peak with prominent interference fringes; Fig. 3 shows subsets of the CL hyperspectral image. Each spatial pixel in this dataset contains a full 1024-point CL spectrum, to which a single Gaussian peak was fitted using a non-linear least squares (NLLS) algorithm. The maps show each of the three fitting parameters thus extracted, namely the peak height, peak energy and full width at half maximum (FWHM). The effects of the composition variation on the emission characteristics are clearly seen, with lower energy, broader peaks featured in the more indium rich regions of the wafer.

Statistical correlations between the various measurements can be examined using 2-dimensional histograms, or correlation plots, as illustrated in Fig. 4. Each of these plots combines the data from two maps, with the value of each pixel on the first map plotted against the value of the corresponding pixel in the second. Since the most significant effect of the variation in substrate temperature (T) is on the incorporation of indium into the epilayers, and since no direct measure of T is available, the InN fraction will be taken as the "independent" variable in this analysis. A clear negative correlation can be observed between the GaN and InN fractions, as evidenced by the sloping shape to the data in Fig. 4(a). No such pattern is observable between the AlN and InN fractions (Fig. 4(b)) or the plot of Al:Ga ratio as a function of InN (Fig. 4(c)), whilst a very strong correlation is seen in the plot of CL peak energy vs. InN.

In order to draw more quantitative conclusions about the degree of correlation between the maps, the Pearson product-moment correlation coefficients (r) have been calculated. These coefficients

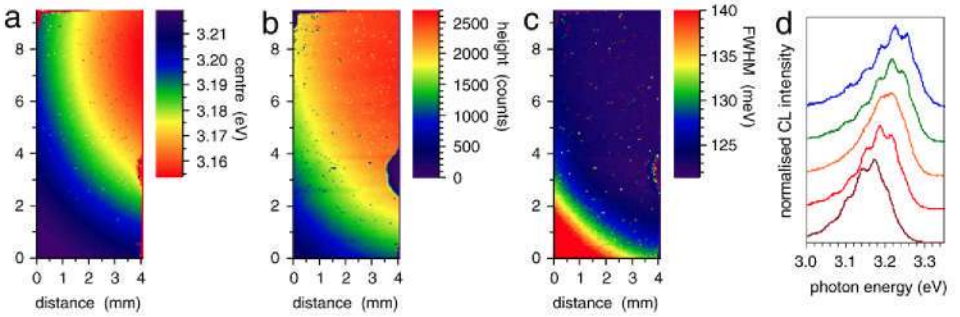

Fig. 3. Maps resulting from non-linear least squares fitting of a single Gaussian peak to the hyperspectral CL dataset, showing (a) peak energy, (b) relative peak height and (c) peak FWHM, with sample spectra (d).

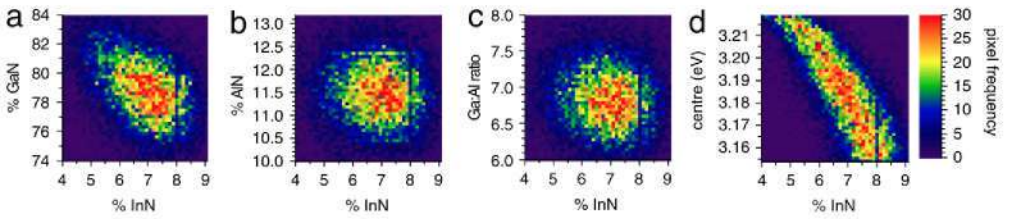

Fig. 4. 2-dimensional histograms correlating the data from Figs. 1 and 3, showing (a) the GaN fraction, (b) the AlN fraction, (c) the Ga:Al ratio and (d) the CL peak energy, each as a function of InN content.

Table 1
Summarised correlation data.

Correlated data	Pearson coefficient (r)
InN (%) vs. GaN (%)	−0.40
InN (%) vs. AlN (%)	−0.08
InN (%) vs. Ga:Al atomic ratio	−0.10
InN (%) vs. CL peak energy (eV)	−0.75

would give values of +1(−1) for perfect positive (negative) linear correlations and a value of 0 for no linear correlation. The Pearson coefficients calculated for each of the plots in Fig. 4 are shown in Table 1.

Previous data obtained from measurements on multiple samples (and therefore with larger variation in both growth temperature and composition) from the same series of growth runs showed significant trends over the set [3]. Comparison of those results with the current work allows the significance of the trends seen here (and hence the significance of a given correlation coefficient) to be tested.

The correlation between the InN fraction and the CL peak energy is strong, as seen in Fig. 4(d), and has a correspondingly high r value of −0.75. The InN vs. GaN plot (Fig. 4(a)), shows a dependence that, whilst weaker at $r = -0.40$, is still clearly correlated. The relationship between InN and AlN is much less evident from inspecting either the maps (Fig. 1(a) vs. 1 c) or the associated correlation plot (Fig. 4(b)). However, a weak negative correlation can be discerned, for example from the plot in Fig. 2, and is confirmed by the analysis reported for the multiple-sample data [3]. Thus we contend that the r value of −0.08, whilst close to zero, is still sufficient to indicate an underlying correlation beneath the noise. Similarly, the Ga:Al ratio, which again showed little evidence of systematic variation with InN by inspection of the correlation plot (Fig. 4(c)), has a negative Pearson coefficient of a similar scale ($r = -0.10$); this too is confirmed in the multiple-sample data, in which this unexpected variation in Ga:Al ratio with In content was observed. Hence, these data suggest that significance can be attributed

to Pearson correlations at least as low as 0.08, even though a value of 0 formally equates to the absence of a linear correlation.

5. Conclusions

By mapping elemental composition across a sufficiently large area ($\approx$30 mm^2) of a single PA-MBE grown AlInGaN epilayer, we have shown that it is possible to make use of composition variations arising from growth temperature gradients to probe the interdependence of AlN, InN and GaN in the material. By combining this with simultaneously-acquired CL emission data, and looking at statistical trends in the data, similar results have been obtained to those from studies involving whole series of many systematically varied samples. The results are used to consider the significance of the Pearson coefficients computed from various correlation plots.

Acknowledgments

The Strathclyde work acknowledges funding from the UK EPSRC through III-N Platform Grants. This work was also partially supported by research grants from the Spanish Ministry of Education (MAT2004-2875, NAN04/09109/C04/2, Consolider-CSD 2006-19, and FPU program); and the Community of Madrid (GR/MAT/0042/2004 and S-0505/ESP- 0200).

References

[1] M.E. Aumer, S.L. LeBoeuf, F.G. McIntosh, S.M. Bedair, Appl. Phys. Lett. 75 (1999) 3315.
[2] J. Li, K.B. Nam, K.H. Kim, J.Y. Lin, H.X. Jiang, Appl. Phys. Lett. 78 (2001) 61.
[3] K. Bejtka, P.R. Edwards, R.W. Martin, S. Fernández-Garrido, E. Calleja, J. Appl. Phys. 104 (2008) 073537.
[4] S. Fernández-Garrido, J. Pereiro, F. González-Posada, E. Muñoz, E. Calleja, A. Redondo-Cubero, R. Gago, J. Appl. Phys. 103 (2008) 046104.
[5] S. Fernández-Garrido, A. Redondo-Cubero, R. Gago, F. Bertram, J. Christen, E. Luna, A. Trampert, J. Pereiro, E. Muñoz, E. Calleja, J. Appl. Phys. 104 (2008) 083510.
[6] R.W. Martin, P.R. Edwards, K.P. O'Donnell, M.D. Dawson, C.W. Jeon, G.R. Rice, I.M. Watson, Phys. Stat. Sol. (A) 201 (2004) 665.
[7] R.W. Martin, P.R. Edwards, K.P. O'Donnell, E.G. Mackay, I.M. Watson, Phys. Stat. Sol. (A) 192 (2002) 117.